Perphenazine-Macrocycle Conjugates Rapidly Sequester the Aβ42 Monomer and Prevent Formation of Toxic Oligomers and Amyloid

Sarah R. Ball[1], Julius S. P Adamson[2], Michael A. Sullivan[1], Manuela R. Zimmermann[3], Victor Lo[1], Maximo Sanz-Hernandez[4], Xiaofan Jiang[2], Ann H. Kwan[5], André D. J. McKenzie[2], Eryn L. Werry[2, 6], Tuomas P. J. Knowles[3, 7], Michael Kassiou[2], Georg Meisl[3], Matthew H. Todd[8*], Peter J. Rutledge[2*] and Margaret Sunde[1*]

[1]School of Medical Sciences, The University of Sydney, Sydney, New South Wales 2006, Australia. [2]School of Chemistry, The University of Sydney, Sydney, New South Wales 2006, Australia. [3]Centre for Misfolding Diseases, Yusuf Hamied Department of Chemistry, University of Cambridge, Cambridge, CB2 1EW, UK. [4]Department of Life Sciences, Imperial College London, South Kensington, SW7 2AZ, UK. [5]School of Life and Environmental Sciences, The University of Sydney, Sydney, New South Wales 2006, Australia. [6]Brain and Mind Centre, The University of Sydney, New South Wales 2006, Australia. [7]Cavendish Laboratory, University of Cambridge, Cambridge, CB3 0HE, UK. [8]School of Pharmacy, University College London, London, WC1N 1AX, UK.

*Co-corresponding authors: Margaret Sunde, Peter Rutledge, and Matthew Todd

Email: margaret.sunde@sydney.edu.au; peter.rutledge@sydney.edu.au; matthew.todd@ucl.ac.uk

Keywords

amyloid, Alzheimer's disease, monomer sequestration, oligomers, inhibition, kinetic analysis

Abstract

Alzheimer's disease is imposing a growing social and economic burden worldwide and effective therapies are urgently required. One possible approach to modulation of the disease outcome is to use small molecules to limit the conversion of monomeric amyloid (Aβ42) to cytotoxic amyloid oligomers and fibrils. We have synthesized modulators of amyloid assembly that are unlike others studied to date: these compounds act primarily by sequestering the Aβ42 monomer. We provide kinetic and NMR data showing that these perphenazine conjugates divert the Aβ42 monomer into amorphous aggregates that are not cytotoxic. Rapid monomer sequestration by the compounds reduces fibril assembly, even in the presence of pre-formed fibrillar seeds. The compounds are therefore also able to disrupt monomer-dependent secondary nucleation, the autocatalytic process that generates the majority of toxic oligomers. The inhibitors have a modular design that is easily varied, aiding future exploration and use of these tools to probe the impact of distinct Aβ42 species populated during amyloid assembly.

Introduction

Alzheimer's disease (AD) is the most common form of dementia and one of the most devastating diseases of the current age. The limited functional improvement in patients treated with antibodies that bind fibrillar forms of the amyloid-β peptide (Aβ) requires that the search for effective therapies continue. Amyloid formation by Aβ is a complex, multiple-step process, initiated by primary nucleation from Aβ monomers. This is followed by recruitment of additional monomers, leading to the formation of multiple different soluble oligomers with a range of sizes and toxicities[1-3]. Although the full sequence of critical molecular events that lead to neuronal death is yet to be defined, this self-assembly of Aβ into soluble oligomers has been shown to generate neurotoxic oligomeric species[4-6]. These oligomers impact neuronal activity through effects on cell membranes, calcium homeostasis, mitochondrial remodelling and glutamate reuptake, amongst other deleterious mechanisms[7-11]. As fibrils form, they offer sites for elongation at their ends, and for secondary nucleation on their lateral surfaces[12, 13], generating further oligomeric species. Secondary nucleation is a significant source of cytotoxic oligomeric Aβ42 species and is the dominant nucleation process in cerebrospinal fluid and in the presence of phospholipid membranes[14].

Effective inhibition of Aβ-associated toxicity is likely to require a mechanism that is effective against all steps of the pathway[15, 16]. Several small molecules or peptides have been shown to suppress primary nucleation or to accelerate fibril formation[17-20] and have shown promise in animal models, but are yet to show efficacy in clinical trials[21]. Some small molecules increase the population of neurotoxic Aβ oligomers[22] and other proposed inhibitors are not effective in the presence of pre-formed fibrils[2, 17]. Molecular chaperone domains and certain antibody fragments are inhibitors of secondary nucleation[23, 24], as are some small molecules[19, 25]. Progress towards the identification of effective modulators of the Aβ assembly process has been slowed by the use of poorly characterised preparations of the peptide and by testing against Aβ40, the less amyloidogenic and less clinically relevant isoform, rather than Aβ42[26-28].

We have shown previously that cyclam derivatives with triazole-linked pendant groups can adopt a range of different, defined pendant geometries depending on the connectivity of the triazole linker and the metal ion coordinated by the macrocycle[9, 29, 30]. Combining these insights with the documented capacity of polymeric perphenazine conjugates to modulate Aβ aggregation[28], we designed a series of molecules in which cyclam is linked via click-derived triazoles to pendant groups that are known to interact with Aβ42.

Quantitative kinetic analyses demonstrate that this series of molecules effectively and rapidly sequesters the monomeric form of Aβ42. We show that this monomer sequestration activity inhibits downstream events that are dependent on monomer concentration. This includes the formation of toxic oligomers and amyloid fibril assembly; the latter is suppressed even in the presence of preformed fibril seeds. These novel molecules redirect the Aβ42 formation pathway towards the generation of amorphous aggregates that are not toxic to differentiated, neuron-like SH-SY5Y cells. This study provides the first demonstration of a reduction in neurotoxicity resulting from the designed diversion of the Aβ42 monomer into non-toxic assemblies.

Results and Discussion

Perphenazine-cyclam conjugates inhibit Aβ42 amyloid assembly

A series of cyclam conjugates was designed to enable a systematic investigation of the Aβ aggregation and amyloid assembly pathways. Six parent cyclam derivatives were prepared: the mono-substituted naphthyl (**C1**), dopamine (**C4**) and perphenazine (**C7**) analogues, and corresponding bis-substituted compounds with naphthyl (**C10**), dopa (**C13**) and perphenazine (**C16**) pendants, along with their zinc(II) and copper(II) complexes (mono-naphthyl **C2**, **C3**; mono-dopa **C5**, **C6**; mono-perphenazine **C8**, **C9**; bis-naphthyl **C11**, **C12**; bis-dopa **C14**, **C15**; and bis-perphenazine **C17**, **C18**) (Fig. 1A and SI Fig. S1A).

Initial screening of these compounds showed the bis-perphenazine derivative (ligand **C16**) to have the most promising capacity to suppress amyloid formation by Aβ42, the isoform of amyloid-β that is clinically associated with an increase in amyloid deposition[31] (SI Fig. S1B).

We prepared the bis-perphenazine ligand (**C16**) and its zinc (**C17**) and copper (**C18**) complexes (Methods, Scheme 1) and characterised the inhibitory activity of these compounds against highly purified, monomeric recombinant Aβ42, prepared using the methods of Linse and colleagues[32, 33]. Aβ42 prepared according to these protocols displays highly reproducible kinetics of amyloid assembly and the three cyclam conjugates **C16**, **C17** and **C18** were found to be potent inhibitors of Aβ42 amyloid fibril formation, as monitored by ThT fluorescence (Fig. 1; SI Fig. S2–S4).

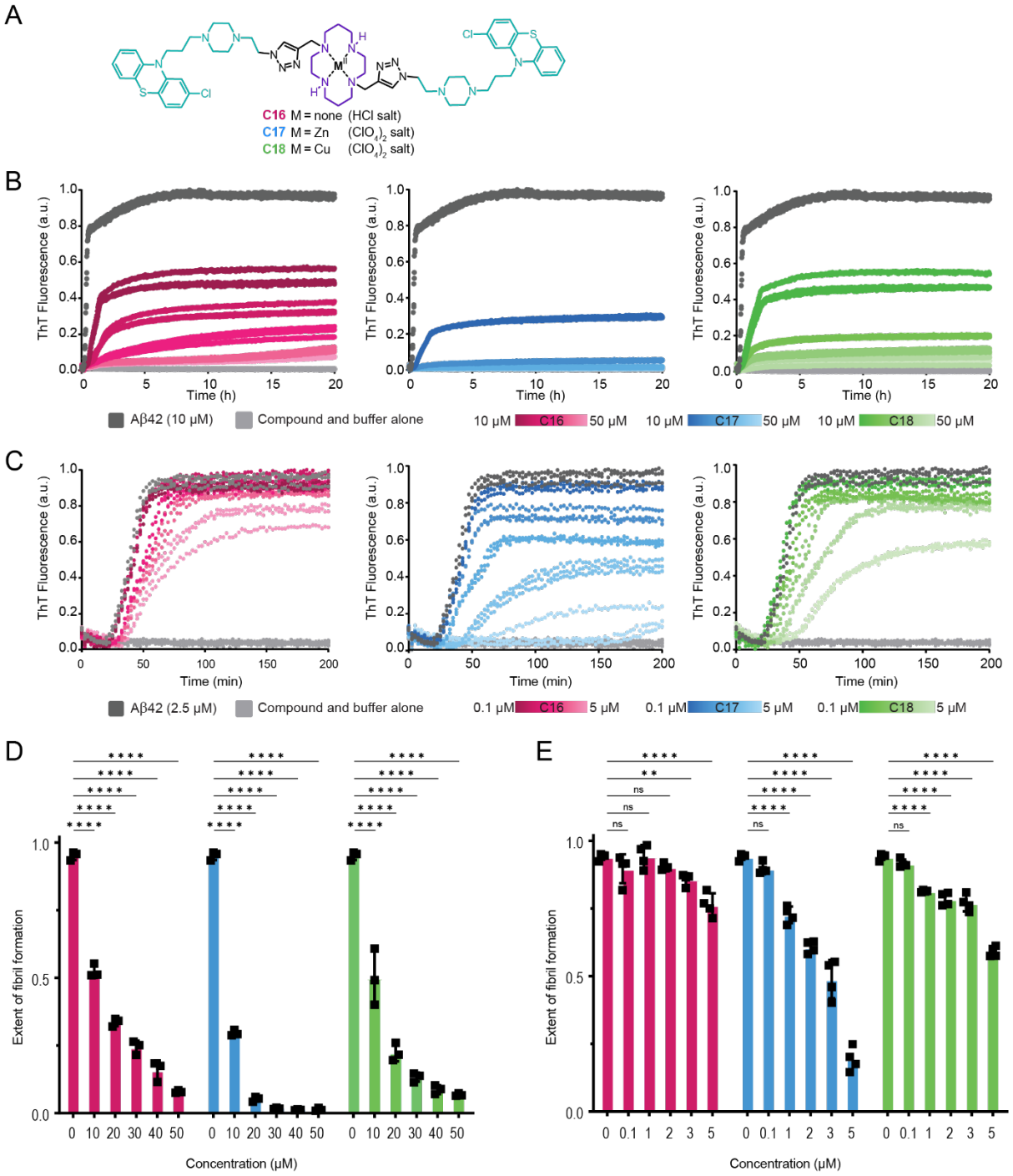

Fig. 1. Concentration-dependent inhibition of Aβ42 fibril formation by macrocycle conjugates C16, C17 and C18. *(A)* The compounds combine a cyclam macrocycle (purple) with pendant

perphenazine moieties (cyan), conjugated via a click-derived triazole (black), and deployed either as the unmetallated HCl salt **C16**, the zinc (II) perchlorate complex **C17**, or the copper(II) perchlorate **C18**. *(B)* 10 μM Aβ42 in 1% DMSO (dark grey) or in the presence of 10–50 μM of **C16** (pink), **C17** (blue) and **C18** (green). N = 3 (SI Fig. S2). *(C)* 2.5 μM Aβ42 in 1% DMSO (dark grey) or in the presence of 0.1–5 μM of compounds. N = 4 (SI Fig. S3). Traces have been baseline-corrected for time zero and adjusted to a scale where the maximum ThT intensity observed from the Aβ42-only sample is 1. Extent of amyloid fibril formation as a function of indicated conjugate concentration with *(D)* 10 μM or *(E)* 2.5 μM Aβ42. Symbols depict extent of fibril formation across 3 replicates for 10 μM and 4 replicates for 2.5 μM series, error bars indicate mean ± SD. Two-way ANOVA followed by a Tukey's multiple comparison test was used to assess impact of three conjugates on fibril formation over two different ranges of [Aβ42] and [conjugate]. (**** $p < 0.0001$, *** $p < 0.001$, ** $p < 0.01$, ns = non-significant). Full statistical analysis provided in SI Table S1–S4. Analysis and preparation of graph with GraphPad Prism.

The three cyclam conjugates demonstrated a concentration-dependent effect, and with 10 μM Aβ42 and a 1:5 molar ratio of Aβ42:conjugate, amyloid assembly was almost completely suppressed, as judged by the reduction in the level of Thioflavin T (ThT) fluorescence observed (Fig. 1B). Assays at 2.5 μM Aβ42, using a range of concentrations that allowed the plateau phase of amyloid assembly to be reached, revealed that all three compounds also introduce an increase in the length of the lag phase (Fig. 1C). Significant inhibition was observed in the presence of the zinc(II) complex **C17** and the copper(II) complex **C18** at concentrations as low as 1 μM with 2.5 μM Aβ42 but only above 3 μM with the uncomplexed ligand **C16** (Fig. 1D, E; Fig. S4 and full statistical analysis in SI Tables S1–S4). This highlights the capacity of the central metal ion to influence the relative orientation of the two pendant groups[25, 29, 30] and the three-dimensional shape of the conjugate – and the resulting interaction with Aβ42. The exact nature of the inferred variation in shape between **C16**, **C17** and **C18** remains to be elucidated.

Perphenazine or cyclam alone do not cause strong inhibition of Aβ42 amyloid formation under these conditions, highlighting the fact that it is not the perphenazine or cyclam moieties *per se* that are responsible for the inhibitory activity (SI Fig. S1B, S5A, S5B). Consistent with the observation that perphenazine alone has a small effect on final ThT intensity, Aβ42 incubated in the presence of perphenazine formed abundant short fibrils that were observed in dense bundles (SI Fig. S5B). The observed inhibition of Aβ42 amyloid formation is also not due to an effect of unchelated metal ions directly on Aβ42. Many studies have demonstrated that Zn(II) and Cu(II) cations can themselves inhibit Aβ42 amyloid formation[34-36] and we observe this effect when these cations are added to the assembly reactions, reflected by an increase in the lag phase or a decrease in the observed ThT intensity (SI Fig. S6A, B). However, we observed that **C17** and **C18** remain effective inhibitors of Aβ amyloid formation even in the presence of a large molar excess of the chelating agent EDTA that is sufficient to sequester any free metal ions (SI Fig. S6C).

The perphenazine conjugates divert Aβ42 from amyloid assembly towards amorphous aggregates

A sensitive protein concentration assay confirmed that when the plateau of amyloid assembly was reached, in samples containing Aβ42 only or Aβ42 plus a 5-fold molar excess of conjugate, little Aβ42 remained in solution; instead, the Aβ42 was in an insoluble form that was readily pelleted by centrifugation (SI Fig. S7). Transmission electron microscopy was used to examine the morphology of the Aβ42 material present after incubation with these compounds. A shift from the characteristic fibrillar morphology of Aβ42 amyloid (Fig. 2A) to an amorphous form was observed when the peptide was incubated with **C16**, **C17** or **C18** for 24 or 40 hours (Fig. 2B–I). Although a small amount of fibrillar material was observed on some of the microscopy grids, most of the aggregated material was amorphous. The amorphous aggregates had a beads-on-a-string appearance, with the "beads" approximately 20 nm wide and the "strings" >1 μm in length.

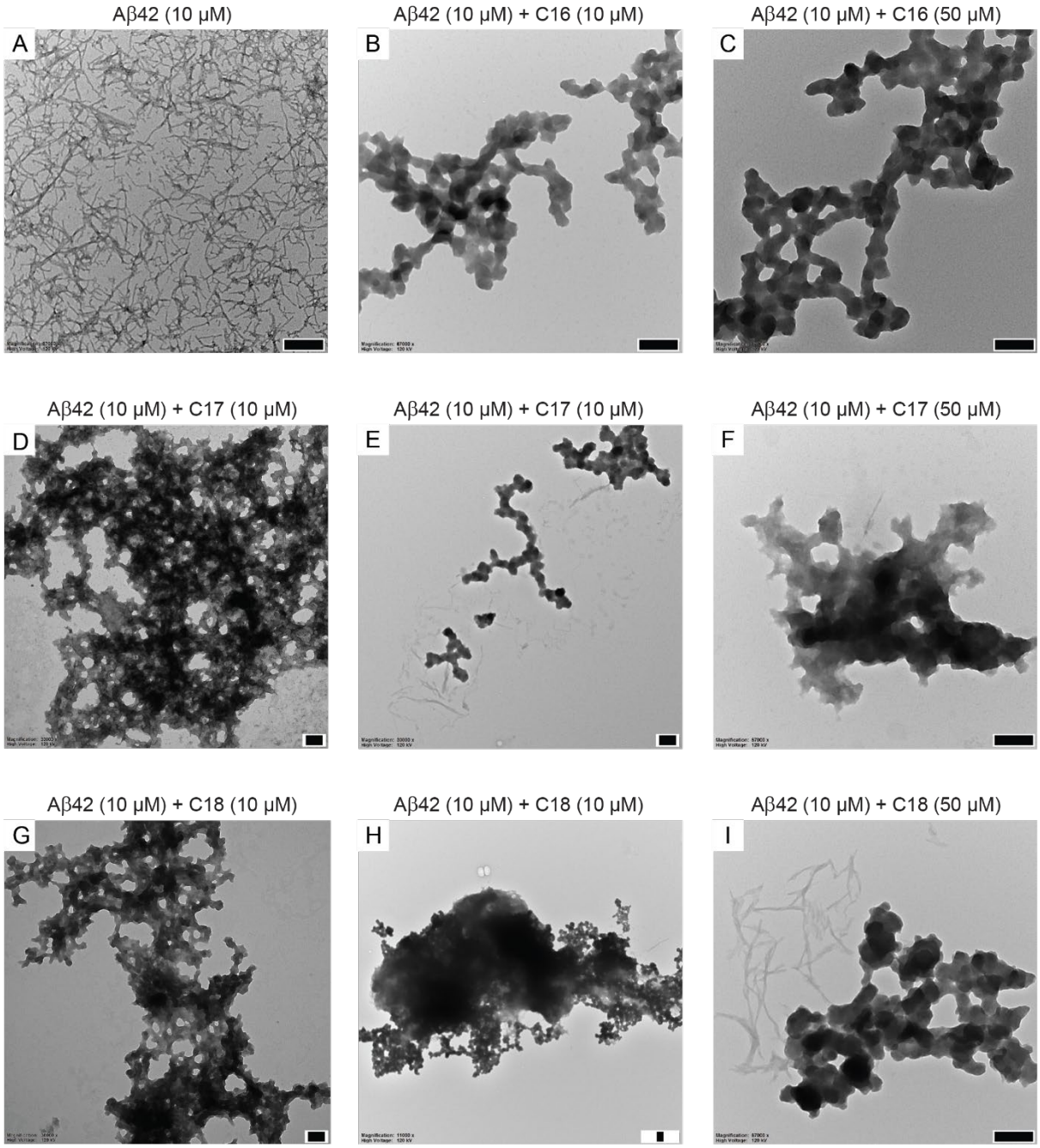

Fig. 2. Conjugates sequester Aβ42 into amorphous aggregates. Transmission electron microscopy images showing representative examples of *(A)* fibrils formed by 10 μM Aβ42 alone, or assemblies formed by 10 μM Aβ42 in the presence of *(B)* 10 μM or *(C)* 50 μM **C16** after 40 h, *(D)* 10 μM **C17** after 24 h, *(E)* 10 μM or *(F)* 50 μM **C17** after 40 h, *(G)* 10 μM **C18** after 24 h, *(H)* 10 μM *or (I)* 50 μM **C18** after 40 h. Black scale bar represents 200 nm.

The perphenazine conjugates reduce cytotoxicity associated with Aβ oligomers

Many groups have demonstrated that soluble intermediate species formed by Aβ42 *in vitro* are neurotoxic[1, 5, 37, 38]. Accordingly, the effect of administration of compounds **C16**–**C18** alone, or co-administration with monomeric or fibrillar Aβ42, was investigated using SH-SY5Y cells which had been differentiated to an AD-appropriate phenotype by treatment with retinoic acid and brain-derived neurotrophic factor[39]. Monomeric Aβ42 was prepared by dissolving in PBS, before being diluted in cell media with or without conjugates and added immediately to cells. Aβ42 fibrils were prepared by incubating the monomeric Aβ42 solution in cell media at 37 °C for 24 hours, a time point significantly past the plateau level in unshaken ThT experiments using cell media (SI Fig. S7A) and then mixing with DMSO or compounds **C16**–**C18** prepared in DMSO. Cells treated with monomeric Aβ42 alone exhibited a highly contrasted and rounded morphology compared to the normal flat morphology observed on control DMSO-treated cells and cells treated with fibrillar Aβ42 alone (SI Fig. S7B,C&D). After 24 hours, the number of metabolically-active cells was measured using a CellTiter-Blue (CTB) fluorescence assay. The CTB assay of cell viability was chosen, given published concerns regarding the use of MTT with Aβ42[1]. These experiments were performed using multiple batches of Aβ42 and consistent inter-batch results were obtained.

By themselves, compounds **C16**, **C17** and **C18** displayed no significant toxicity towards differentiated SH-SY5Y cells, relative to vehicle only (Fig. 3A, ANOVA $F_{(6, 23)} = 7.8$). Exposure of these cells to freshly prepared monomeric Aβ42 resulted in significant ($P < 0.001$) toxicity compared to vehicle, as expected due to the generation of oligomeric species while co-administration with **C16**, **C17** or **C18** resulted in significant protection against this cytotoxicity (Fig. 3B, ANOVA $F_{(6, 23)} = 7.6$). Perphenazine was not cytotoxic by itself and imparted a similar level of protection as **C16**, **C17** and **C18**. The well-studied catechin epigallocatechin gallate (EGCG) provided reduced protection against the cytotoxicity induced by addition of monomeric Aβ42 (Fig. 3A,B), consistent with the level of inhibition of Aβ42 amyloid formation observed in the presence of EGCG (SI Fig. S5C). When Aβ42 was prepared in fibrillar form and then added to cells, no cytotoxicity was observed with fibrils alone or in the presence of compounds (Fig. 3C ANOVA $F_{(6, 23)} = 1.4$).

Following from these experiments, independent concentration response assays were performed with **C16**. The IC_{50} for **C16** was determined to be 2.3 μM (n = 3; SD = 0.9, 95% CI 0.1-4.5) (Fig. 3D). These results demonstrate that the reduction of Aβ42 fibril formation and the diversion of Aβ42 into amorphous aggregates in the presence of **C16**–**C18** is associated with a decrease in the formation of species that are toxic to differentiated SH-SY5Y cells.

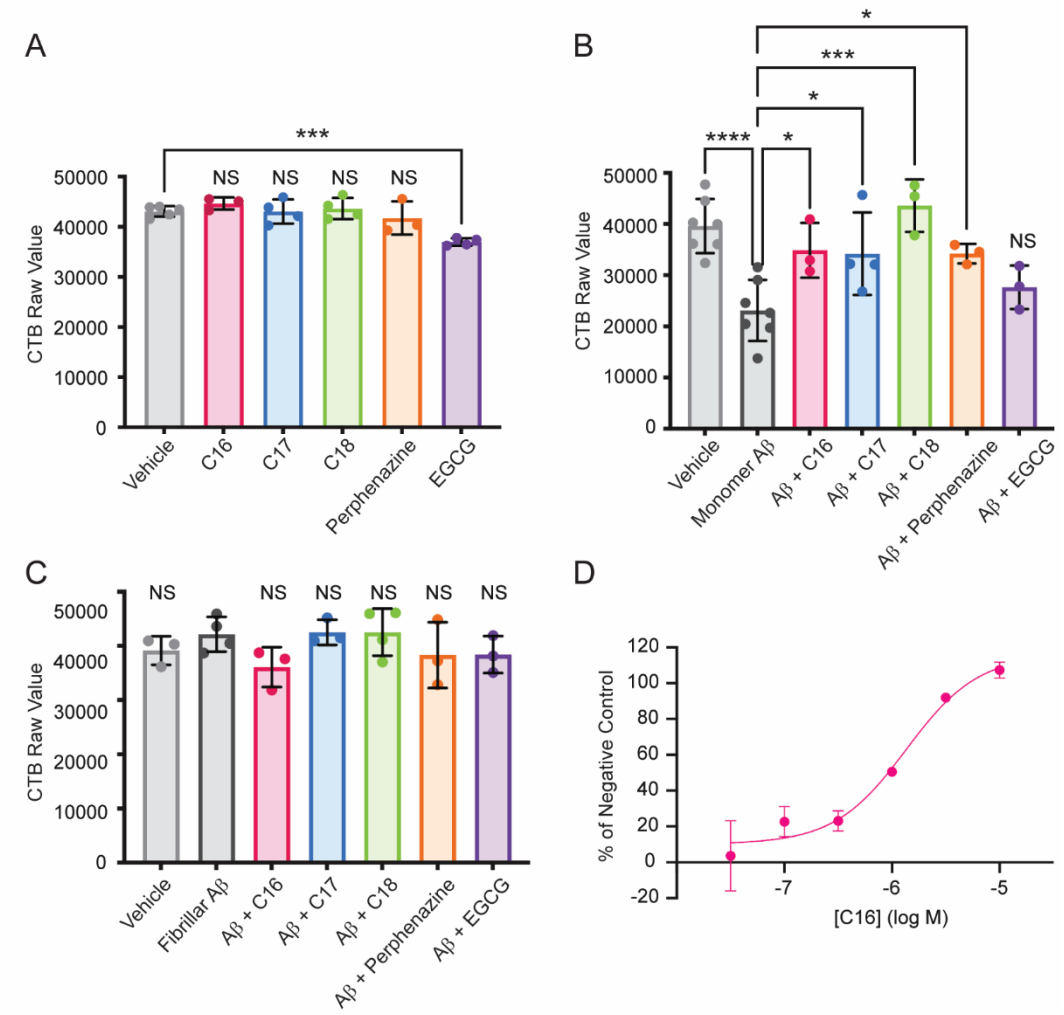

Fig. 3. Decreased formation of cytotoxic species in the presence of perphenazine conjugates. Cell viability was measured using the CellTiter-Blue assay after 24 h incubation with vehicle or 10 μM compound, with or without 20 μM Aβ42. (*A)* Administration of compounds alone. *(B)* Administration of monomeric Aβ42 in the absence or presence of C16–C18, perphenazine and EGCG. *(C)* Administration of fibrillar Aβ42 in the absence or presence of C16–C18, perphenazine and EGCG. The figure displays the mean ± SD of N ≥ 3 independent experiments. One-way ANOVA followed by a Bonferroni's multiple comparisons test at the 0.05 level was used to determine the difference between each condition and vehicle control for the compounds alone or monomeric/fibrillar Aβ42 (**** $p < 0.0001$, *** $p < 0.001$, * $p < 0.05$, NS = non-significant). *(D)* Concentration-response curve for **C16** incubated with Aβ42 showing mean ± SD. IC_{50} = 2.3 μM (SD = 0.9, 95% CI 0.1-4.5). N = 3. Details of statistical analysis in SI Tables S5–S7.

These compounds inhibit Aβ amyloid formation through sequestration of Aβ42 monomers

The microscopic processes underlying amyloid formation of Aβ42 are primary nucleation, elongation and secondary nucleation[40, 41]. Their relative contribution to amyloid assembly can be quantified through their rate constants, obtained by fitting integrated rate laws within the framework of chemical kinetics[42]. ThT fluorescence data measured at 2.5 μM and 10 μM Aβ42, in the presence of a range of cyclam conjugate concentrations, were analysed using the online fitting software AmyloFit. The rate constants of the unperturbed systems agreed well with similar experiments[12] (SI Table S12). To probe the mechanism of action of inhibitory compounds **C16**, **C17** and **C18**, we systematically varied either one rate constant in the rate laws, or the level of available monomer[42]. By comparing how well these modified rate laws describe the data, mechanistic insight can be gleaned. In this way, a mechanism that primarily involves inhibition of primary nucleation could be ruled out for **C16**, **C17** and **C18** as the

origin of the changes in the kinetic behaviour in the presence of the inhibitor (Fig. 4A, C, and all conjugates in SI Fig. S9–13, SI Table S9). However, the fit to the kinetic profiles indicated that inhibition through monomer sequestration is a plausible mechanism (Fig. 4B and C, and SI Fig. S9–13, SI Table S9).

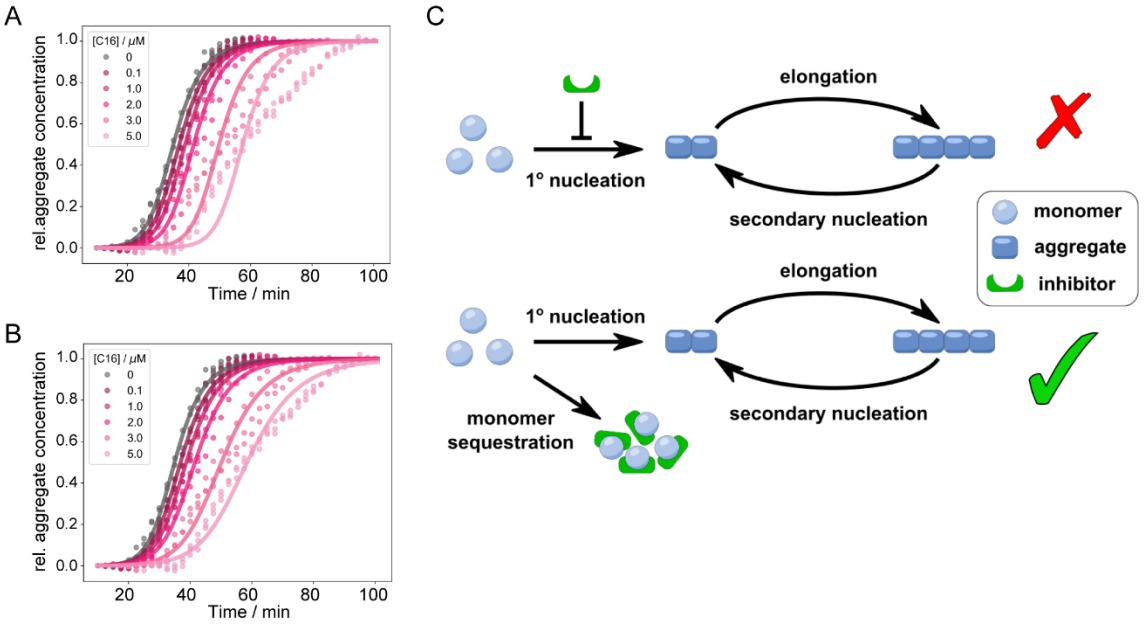

Fig. 4. Kinetic analysis reveals that Aβ42 monomer sequestration by C16–C18 effectively inhibits primary nucleation, secondary nucleation, and elongation. To elucidate the major mechanism of inhibition, normalised aggregation curves measured in thioflavin T fluorescence assays were fitted under the constraint that deviation from the unperturbed system was allowed in only one microscopic step or the free monomer concentration, respectively. Representative curves for **C16** shown in A and B, all fits for all conjugates shown in the SI. *(A)* The observed inhibition cannot be described through inhibition of primary nucleation. *(B)* Inhibition through monomer sequestration is a plausible mechanism based on the kinetic profiles. *(C)* Microscopic steps underlying amyloid formation, with the suggested mode of inhibition through monomer sequestration.

The mechanism of interaction with the conjugates was further probed by the addition of seeds to the assembly reactions. The introduction of small numbers of preformed fibril seeds at the beginning of the fibril assembly reaction can be used to bypass primary nucleation. Notably, the cyclam conjugates remain effective as inhibitors of Aβ42 amyloid fibril formation even when exogenous fibril seeds are present (Fig. 5A B, C). In the presence of 2% or 5% seeds, inclusion of **C16–C18** at 1:2.5 or 1:5 Aβ42:compound molar ratio resulted in inhibition of Aβ42 assembly, with the level of inhibition similar to that observed in the absence of pre-formed seeds (Fig. 5 and SI Fig. S14). In addition to ruling out the blocking of primary nucleation as the source of the inhibitory effect, the results observed in the presence of seeds, when the aggregation reaction reaches completion much sooner, suggest that binding of the compounds to the monomeric form of Aβ42 occurs rapidly on the time scale of aggregation.

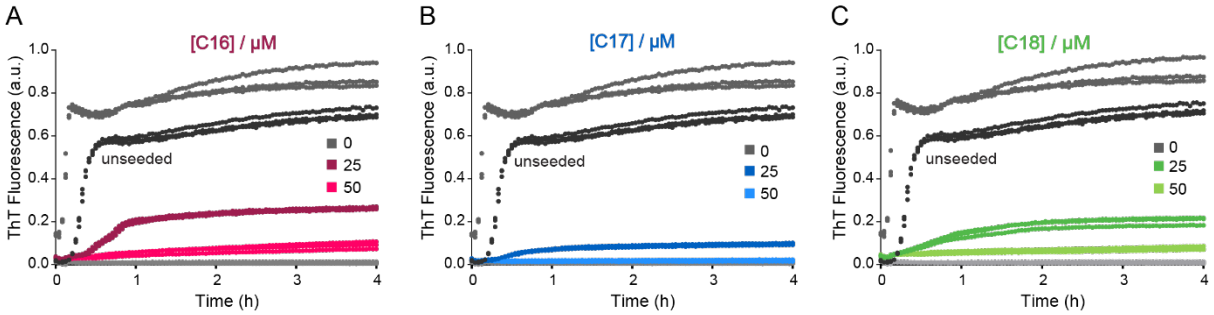

Fig. 5. Cyclam conjugates effectively inhibit fibril formation in the presence of seeds. 10 μM Aβ42, in the absence of seeds (black) or presence of 5% seeds and 1% DMSO (grey), 25 or 50 μM *(A)* **C16**, (B) **C17**, and (C) **C18**. N = 3 (SI Fig. S14). All samples were measured in triplicate under quiescent conditions at 37 °C. Traces have been corrected for time zero and data adjusted to a scale where the maximum ThT intensity observed in the absence of inhibitor is 1, using GraphPad Prism.

Based on the fits to the normalised kinetic data alone, mechanisms based on inhibition of secondary nucleation, inhibition of elongation, and monomer sequestration, were observed to be similarly likely as the main modes of action of compounds **C16**–**C18** (SI Fig. S9–13, SI Table S9). However, we found a clear correlation between the ThT intensity at completion of the aggregation reaction, and the effective monomer concentration determined from the fits (Fig. 6A, B, C insets; SI Tables S10–S12). As the fitting was performed on normalised kinetic data, these two quantities constitute independent measures of the same physical property. This correlation between an equilibrium measure (the plateau level), and a parameter estimated on the basis of normalised kinetics (the effective monomer concentration), provides support for monomer sequestration by these compounds. In addition to accounting for the delay in aggregation and decrease in ThT signal, monomer sequestration by the cyclam conjugates also provides a mechanistic explanation for the appearance of amorphous material described above. These fits were made assuming that this monomer sequestration proceeds much faster than aggregation and can thus be modelled by a reduced effective monomer concentration.

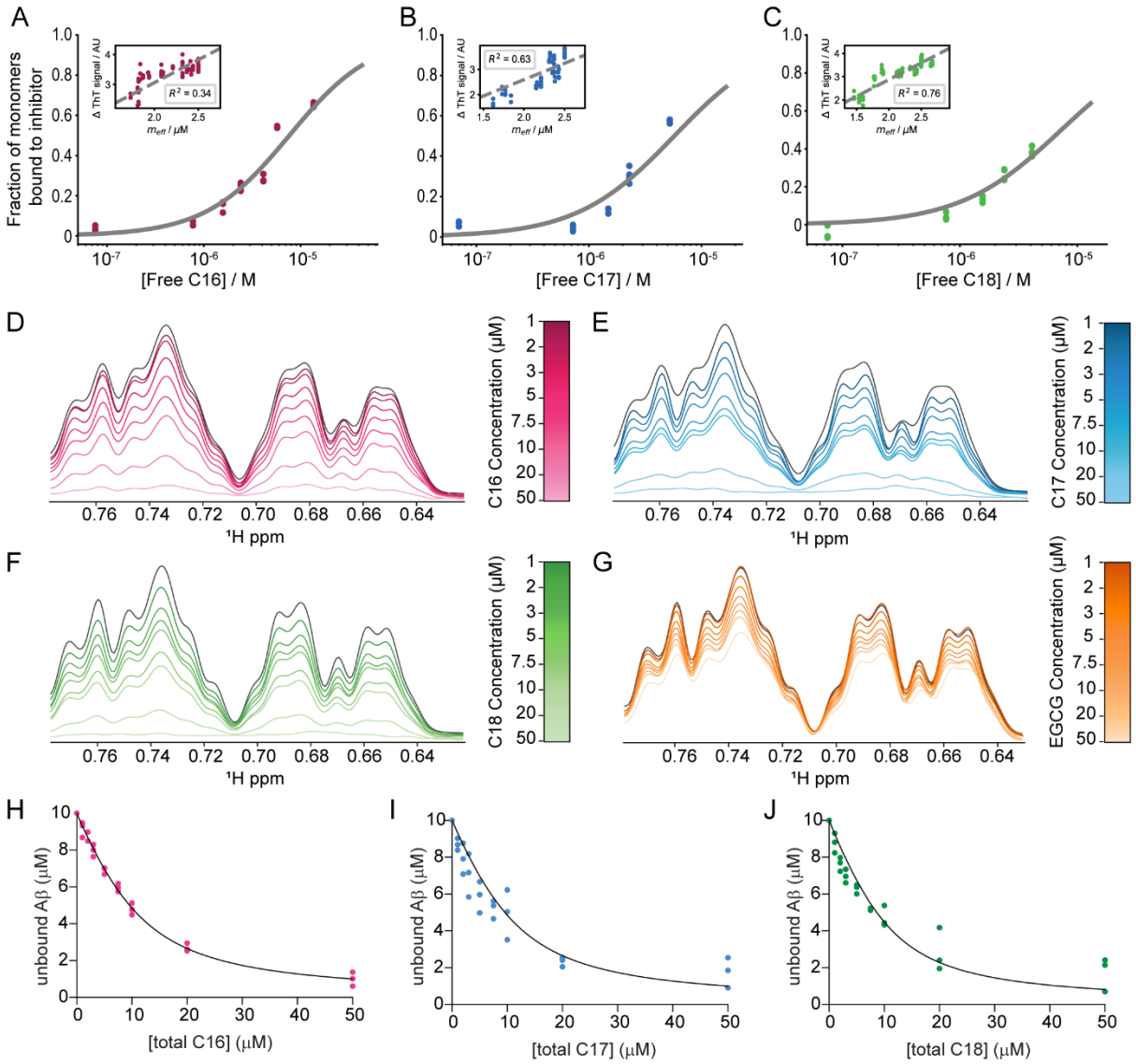

Fig. 6 Effect of conjugates on Aβ42 monomer in solution. Monomer-inhibitor binding curves for *(A)* **C16**, *(B)* **C17** and *(C)* **C18**, with correlation between the effective free monomer concentration, determined by chemical kinetics, and the absolute increase in ThT signal shown as insets (SI Table S10–S12). One-dimensional ^{1}H NMR spectroscopy was used to determine apparent K_D for compounds. Unlabelled 10 μM Aβ42 (dark grey) was incubated with 1–50 μM *(D)* **C16**, *(E)* **C17**, *(F)* **C18** and *(G)* EGCG, and spectra recorded at 4 °C. Methyl proton region is displayed, all regions analysed are shown in SI Fig. 15. Increasing concentration of **C16**–**C18** resulted in a decay in protein signal intensity. Binding curves for *(H)* **C16**, *(I)* **C17** and *(J)* **C18** constructed from signal decay curves and used to calculate the apparent K_D.

Further support for monomer sequestration as the dominant mode of inhibition of Aβ42 aggregation by **C16**, **C17** and **C18** was gained by obtaining consistent values for the apparent dissociation constant of monomer and inhibitor, K_D, by orthogonal methods. First, the effective monomer concentration obtained through the chemical kinetics analysis at different monomer and inhibitor concentrations was used to construct monomer-inhibitor binding curves (Fig. 6A, B, C). To fit these data, we assumed a simple one-to-one binding, yielding K_D values of 7.6 μM (95% CI, 6.6–9.1) for **C16**, 5.7 μM (95% CI, 4.6–7.1) for **C17** and 7.4 μM (95% CI, 6.2–9.1) for **C18**.

Secondly, we utilised one-dimensional ^{1}H NMR spectroscopy to determine an apparent binding constant for the interaction between the conjugates and Aβ42. For each of **C16**, **C17** and **C18**, the compound was titrated into a solution containing 10 μM unlabelled Aβ42, over the concentration range of 1–50 μM. A decay profile in the protein signal intensity across the spectrum was observed with increasing concentration of all three conjugates (Fig. 6 and SI Fig. S15). A 5:1 ratio of inhibitor:Aβ42 resulted in a reduction of proton signals to baseline, consistent with the sequestration of Aβ42 monomer into very large and/or insoluble assemblies, the precipitation of material during the course of the NMR titrations, and the amorphous aggregates observed by transmission electron microscopy (Fig. 3). The signal decay curves were fitted to a quadratic equation for the calculation of the apparent K_D of each compound, yielding 4.6 μM (95% CI, 3.1–6.5) for **C16**, 3.4 μM (95% CI, 2.2–4.9) for **C17** and 3.7 μM (95% CI, 2.4–5.3) for **C18**. The observed effect of these perphenazine cyclam conjugates on Aβ42 assembly is different to that of the polyphenol EGCG, where the presence of EGCG results in only a small decrease in the intensity of the observed ^{1}H spectrum from monomeric Aβ42, up to 31% signal loss at a 5-fold excess of small molecule (Fig. 6G and SI Fig. S16). This is evidence that binding of monomeric Aβ42 to EGCG is weaker than peptide binding to the macrocycle conjugates.

A monomeric sample of recombinant ^{15}N-labeled Aβ42 was prepared and analysed in the absence and presence of **C16** to probe which regions of the polypeptide are involved in the interaction. The chemical shifts in the ^{15}N HSQC spectrum collected in the absence of any added compound were superimposable upon those reported by others previously for Aβ42 (SI Fig. S16)[43]. Addition of **C16** resulted in an immediate reduction in signal intensity that was uniform across all peaks in the spectrum. Protein that is not sequestered into an amorphous aggregate remains in solution at the 1:1 ratio of protein:inhibitor. No peak-specific changes in signal intensity or chemical shift were detected that could be attributed to binding of **C16** to a distinct region of monomeric Aβ42. Instead, the loss of signal is consistent with the binding of monomer to **C16** resulting in the generation of a conformation that is highly aggregation-prone and rapidly forms large structures, undetectable by solution NMR.

We observed that the cyclam conjugates **C16**–**C18** remain effective inhibitors of Aβ42 amyloid fibril formation in the presence of pre-formed seeds, demonstrating that they are not acting on primary nucleation. The fits to the normalised kinetic data cannot distinguish between mechanisms based on inhibition of secondary nucleation, inhibition of elongation, or monomer sequestration. However, only the last of these is consistent with *all* of the experimental data presented here: ThT fluorescence levels, kinetics measurements, the appearance of amorphous aggregates when compounds bind to Aβ42, and loss of solution NMR signal upon addition of compounds to Aβ42. It is not possible to measure the concentration of the amorphous aggregates directly, hence we are unable to model the formation of these complexes explicitly. We have assumed a 1:1 binding between compounds and Aβ42, however the rapid formation of large aggregates suggests that binding to the conjugates may induce a

conformation in Aβ42 that recruits further molecules from solution. Our data are consistent with Aβ42 binding to the inhibitor quickly but then dissociating slowly from the complex. Comparison of the results presented here, with other studies that have investigated the effect of perphenazine alone on the oligomerisation, fibrillisation and cytotoxicity associated with Aβ, indicate that changes in the pathway of fibril assembly, or the type of oligomers formed by Aβ when it self-assembles, result in alterations in observed cytotoxicity. Perphenazine diverts Aβ42 to a different oligomeric form to that generated by Aβ42 alone, but fibrils are observed to form eventually. Necula and co-workers found that perphenazine changed the size distribution of oligomers and the population detected by the A11 antibody but did not inhibit Aβ42 fibril formation and promoted the rate of formation of some oligomers and, ultimately fibrils[44]. Other studies with perphenazine and the less aggregation-prone Aβ40 have demonstrated that perphenazine slows the formation of nuclei but accelerates conversion of nuclei into fibrils[28]. The perphenazine moiety of the conjugates is likely to interact with Aβ42 in a similar manner to perphenazine only. However, the three-dimensional, multi-arm structure of the conjugates appears to trap the peptide in a large amorphous aggregate and inhibit subsequent conversion of Aβ42 into a fibrillar form. Since toxicity is associated with oligomeric forms, both perphenazine and the conjugates reduce the cytotoxic effect observed when monomeric Aβ42 is applied to cells, however the final self-assembled form of Aβ42 is different.

The ability to interrogate a change in amyloid assembly kinetics and thereby identify the mechanism of inhibition, offers new opportunities to understand the consequences of intervention at defined points within the Aβ42 assembly pathway. The kinetic theory of protein aggregation inhibition reveals that sequestration of monomeric Aβ42 will reduce the rates of primary nucleation, elongation and secondary nucleation, and is therefore likely to have a large impact on amyloid assembly overall[16]. Many studies of peptide-based inhibitors that incorporate “disruption elements” report success in preventing the formation of the β-structure within amyloid fibrils and can influence elongation[45]. Studies of the effect of EGCG on Aβ42 indicate that it converts the peptide to off-pathway oligomers and remodels pre-formed fibrils, although these effects are not rapid[26, 46, 47]. Inhibitors have also been reported that specifically inhibit secondary nucleation[19], but the impact of these interventions on residual Aβ monomer concentration has not always been described. The intrinsically disordered and dynamic nature of monomeric Aβ42 has impeded the use of traditional drug discovery approaches that focus on identifying chemical moieties that bind to defined sites on the target. A small molecule (10074-G5) that binds to the monomeric form of Aβ42 has been reported[2, 3] and the binding of 10074-G5 to Aβ42, with K_D of ~40μM, maintains Aβ42 in a soluble form and reduces its hydrophobicity[48]. 10074-G5 reduces functional deficits in a *C. elegans* model of Aβ42-associated toxicity, however its impact on neuronal toxicity is yet to be reported and it does not display a concentration-dependent inhibition of seeded assembly *in vitro*.

We have designed a class of compounds that predominantly sequester the monomeric form of Aβ42 and direct its assembly into non-fibrillar forms, with associated reduction in the level of cytotoxic species present. The inventive modular design of the compounds described here offers a toolkit for future elucidation of the key moieties and properties that influence Aβ42 monomer binding and subsequent formation of amorphous aggregates. Compounds that sequester monomeric Aβ42 will be needed at relatively high concentrations, therefore further optimisation of affinity, stoichiometry and bioavailability will be required to develop this into a viable therapeutic strategy. Many small molecules have been described as modulators of Aβ42 amyloid assembly and could be incorporated into the design with the aim of increasing the affinity or specificity of the interaction with Aβ42. The number of pendant groups attached to this cyclam scaffold can be increased to four, potentially increasing the number of Aβ42 peptides binding to each conjugate molecule. This scaffold provides a base for future rational design of more potent compounds, with reduced lipophilicity and molecular weight, that act through the same mechanism, yet which are accessible via a divergent synthetic strategy. This class of compounds can provide wide mass-to-charge and hydrophobic-to-hydrophilic surface area ratios, while the attachment of both rigid and flexible pendants provides a great diversity of possible interactions with client protein targets. The switchable geometry allows maintenance of a constant periphery while varying the gross molecular shape. Given that self-assembly and aggregation of proteins are three-dimensional

processes, this level of structural control has significant potential to contribute to effective inhibition. AD is one of over 50 human disorders considered to be proteinopathies. The critical pathogenic species associated with protein aggregation and amyloid formation in each of these disorders likely have unique features. However, a similar dissection of assembly pathways with modular scaffolds decorated with protein-specific binding moieties may reveal points for therapeutic intervention in other protein aggregation-related diseases.

Methods

Synthesis of lead compounds C16–C18.

Full synthetic procedures and characterisation data are detailed in the Supporting Information.

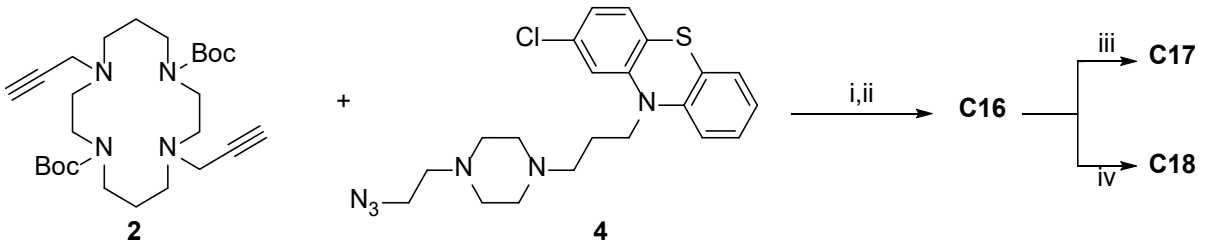

Reaction scheme 1: Cyclam (1,4,8,11-tetraazacyclotetradecane) **1** was converted to the di-Boc-di-propargyl derivative **2** in 68% yield over four steps using previously reported methods[9, 49]. Perphenazine **3** was converted to the azide **4** (79%) by activating its primary alcohol with diphenylphosphoryl azide (DPPA) and displacing with sodium azide in dimethylformamide (DMF). The azide **4** (2 equivalents) and bis-alkyne **2** were coupled using a copper-catalysed azide/alkyne cycloaddition reaction (CuAAC) to yield the protected ligand **5** (46%), before the Boc groups were removed using 4 M HCl in dioxane to afford **C16** (74%). The HCl salt **C16** was converted to its zinc(II) (**C17**) and copper(II) (**C18**) complexes by first treating with Ambersep 900 hydroxide form resin to generate the free amine, then stirring overnight at room temperature with either zinc(II) perchlorate hexahydrate (for **C17**, 63%) or copper(II) perchlorate hexahydrate (for **C18**, 64%). All compounds were dissolved in 100% DMSO and stored at 4 °C until use. Reagents and conditions: i. $CuSO_4.5H_2O$ (0.2 equiv.), sodium ascorbate (0.5 equiv.), THF/H_2O (2:3), rt, 16 h, 46%; ii. 4 M HCl in dioxane (excess), 0 °C, 1 h, 74%; iii. Ambersep 900 hydroxide form resin, MeOH, 15 min, then $Zn(ClO_4)_2$, MeOH, reflux, 16 h, 63%; iv. Ambersep 900 hydroxide form resin, MeOH, 15 min, then $Cu(ClO_4)_2$, MeOH, reflux, 16 h, 64%.

Aβ42 Overexpression and purification. Overexpression and purification of unlabelled Aβ42 was performed according to Walsh and colleagues[33]. Briefly, large cultures of *Escherichia coli* BL21 Gold (DE3) were incubated at 37 °C with shaking, induced with 0.5 mM IPTG and harvested by centrifugation. Purification involved a series of sonication and centrifugation steps followed by resuspension of inclusion bodies in 8M urea. Anion exchange chromatography using diethylaminoethyl cellulose beads was performed and protein eluted with increasing concentrations of NaCl (up to 150 mM). Aβ42 elution was assessed by electrophoresis, using by Novex 10–20% Tricine SDS-PAGE gels. Fractions containing elevated levels of Aβ42 were combined and filtered through a 30 kDa molecular mass cut-off centrifugal filtration device (Amicon Ultra-15). The combined sample was concentrated using a 3 kDa molecular mass cut-off centrifugal filtration device (Amicon Ultra-15), snap frozen, lyophilised and stored at –20 °C. ^{15}N Aβ42 expression was performed according to Habchi and colleagues[19], with purification as above.

Size exclusion chromatography. An aliquot of lyophilised Aβ42 protein was solubilised in 6 M GuHCl until no large aggregates were visible. The sample was centrifuged at ~3300 x *g* for 3 min, bath sonicated for 5 min in ice-water and centrifuged again at 16000 x *g* for 10 min at 4 °C. 500 µL of sample was drawn up carefully with a syringe and loaded onto a Superdex 75 Increase 10/300 GL size exclusion column running on an ÄKTA FPLC system. Protein was eluted at 0.5 mL/min in 50 mM ammonium acetate pH 8.5. Fractions (0.5 mL) were collected in Protein LoBind Eppendorf tubes and immediately placed on ice. Fractions were analysed for Aβ42 content using SDS-PAGE. Concentration was measured via spectrophotometer (ε275 = 1450). Fractions containing Aβ42 were combined and either used immediately or snap frozen and lyophilised.

Thioflavin T assays. Protein samples (Aβ42) were prepared in triplicate in non-binding 96-well half area plates (Corning 3881) in 25 mM or 50 mM NaH_2PO_4 pH 7.4, 40 µM ThT to a final volume of 80 µL. Plate preparation was performed at 4 °C to minimise aggregation. Samples were incubated at 37 °C in a POLARstar Omega microplate reader (BMG Labtech), with excitation at 440 nm and the fluorescence

emission recorded at 480 nm under quiescent conditions. EGCG and perphenazine were purchased from Sigma and Combi-Blocks, respectively. Stock solutions prepared at 2.5 or 5 mM in water (EGCG) and DMSO (perphenazine).

Seeding. Seeds were prepared by incubating 10 μM Aβ42 in 50 mM NaH_2PO_4, pH 7.4 at 37 °C for 5 h. Protein solution was subjected to 6 x 10 s sonication with 20 s rest on ice between cycles. The seeds were maintained on ice and used immediately.

Enhanced BCA assay details. Kinetic assays were run to completion as judged by the plateau in ThT fluorescence (~5 h). Contents of wells were removed and centrifuged at 16000 x *g* for 10 min to pellet fibrils and aggregates. Protein concentration in the remaining supernatant fraction was determined using a Pierce Bicinchoninic Acid Protein Assay Kit according to manufacturer's enhanced protocol. Solutions containing monomeric Aβ42 and compounds alone were used as controls.

TEM. Samples were prepared on carbon-coated copper grids (200 mesh) with formvar support film (ProSciTech Pty Ltd.) that had been exposed to UV light (230 nm) for 10 min before sample application and stained with 2% aqueous uranyl acetate solution. Samples were examined with a FEI Tecnai T12 electron microscope operating at 120 kV and images captured with a Veleta CCD camera and processed using RADIUS 2.0 imaging software (EMSIS GmbH).

Preparation of Aβ42 for cell assay and NMR. Lyophilised, purified protein was resuspended in HFIP at 1 mg/mL and incubated for 30 min at room temperature. The protein was snap frozen, lyophilised, and stored at –80 °C until use.

Cell Culture and Differentiation. SH-SY5Y cells (a kind gift from Prof L. Ittner, Dementia Research Centre, Macquarie University, Australia) were cultured in in Dulbecco's Modified Eagle Medium: Nutrient Mixture F-12 (DMEM/F12; Invitrogen, Carlsbad, CA, USA) supplemented with 10% fetal bovine serum (FBS; Gibco, Uxbridge, UK) at 37 °C and 5% CO_2. Cells were fed every 2-3 days and passaged using Trypsin-EDTA (0.25%). Cells were detached using Trypsin-EDTA, centrifuged (5 min, 125 x *g*), counted and then plated in a Cell-bind 96-well plate at a density of 0.5 x 10^4 cells/well in 10 μM all-trans retinoic acid (RA; Sigma-Aldrich) in DMEM/F12 with 10% FBS. Media was replaced daily for 4 days (RA is light sensitive, so all steps involving RA were completed in the dark). After a 4-day incubation with RA, media was switched to DMEM/F12 (no serum) with 50 ng/mL BDNF (Sigma-Aldrich) for 3 days. After a total of 7 days of differentiation the cells were used for the experiments.

Aβ42 preparation, compound treatment and CellTiter-Blue viability assay. 24 h prior to the cells finishing differentiation, an aliquot of Aβ42 was centrifuged at 16,000 x *g* for 10 min and dissolved in PBS at 200 μM, then diluted to 20 μM in DMEM/F12 with 10% FBS. The solution was stored in the incubator (37 °C, 5% CO_2) in a low-bind Eppendorf to promote Aβ42 fibrillization. After cell differentiation was complete, for the Aβ42 monomeric preparation, a second aliquot of Aβ42 was centrifuged at 16,000 x *g* for 10 min, dissolved in PBS at 200 μM and immediately diluted to a final concentration of 20 μM in DMEM/F12 (with 10% FBS). Experimental compounds (10 μM, 0.1%) or DMSO control were added to the fibrillar or monomeric Aβ42. Differentiation media was aspirated, 100 μL of each condition added to the cells and incubated for 24 h (37 °C, 5% CO_2). In the monomeric preparation, the time between dissolving the Aβ42 and applying onto the cells was minimised (less than 2 min total). After 24 h, CellTiter-Blue (CTB; Promega G8080) (20 μL/well) was added and incubated for 4 h. The fluorescent emission at 590 nm was measured using a POLARstar Omega microplate-reader (BMG Labtech); viable cells metabolise this agent and reduce it to a fluorescent compound. Each condition was plated in duplicate, and data represent the mean of N ≥ 3 independent replicates. Independent concentration response assays were performed with **C16** to determine the IC_{50}. The cells were treated with Aβ42 in the presence of C16 over the range of concentration 0.05–10 μM. Cell viability was measured as described above, N = 3. Multiple batches of recombinant Aβ42 were used for these experiments and gave rise to consistent inter-batch results.

Statistical Analysis. Ordinary one-way ANOVA followed by a Bonferroni's multiple comparisons test with single pooled variance was used to determine the adjusted p-value between mean CTB values of differentiated SH-SY5Y cells treated with Aβ42 and/or test compounds relative to vehicle control. The family-wise alpha threshold and confidence level was set at 0.05 (95% confidence interval). IC50 analysis was conducted using a 4-parameter sigmoidal inhibition dose-response fit in GraphPad Prism 9, with all curves showing a suitable goodness of fit ($R^2 > 0.9$).

Kinetic analysis. The kinetic data obtained in ThT assays were analysed using the online fitting software AmyloFit, following the cited protocol[42]. The model 'secondary nucleation dominated, unseeded' was used, with the reaction orders set to 2 as typical for Aβ42 and under the constraint of allowing deviations from the unperturbed kinetics in only one parameter at a time to investigate which microscopic step or which species of the aggregation mixture was most likely affected by the inhibitors. Repeats of the experiment were analysed separately and combined at the end to estimate uncertainty.

***K_D* determination.** To determine the value of the dissociation constant, K_d, between free monomer and inhibitor, a one-to-one binding was assumed and the free monomer concentration, m, expressed as a function of the total inhibitor concentration, I_{tot}, the total monomer concentration, m_{tot}, and K_d,

$$m = \frac{-I_{tot}+m_{tot}-K_D+\sqrt{(I_{tot}-m_{tot}+K_D)^2+4\,K_D\,m_{tot}}}{2}.$$

The free monomer concentration was estimated as the effective monomer concentration in the kinetic assays or the relative one-dimensional ^{1}H NMR signal, respectively. Likelihoods were calculated using grid approximations, under the assumption of Gaussian noise.

NMR / *K_D* Analysis. All NMR data were collected at 4 °C using unlabelled 10 μM Aβ42 or ^{15}N-labelled Aβ42 in 20 mM NaH_2PO_4 pH 7.0, 10% D_2O, 1 mM DSS. Individual titrations with **C16**, **C17**, **C18** or EGCG were carried out by incubating unlabelled 10 μM Aβ42 with increasing concentrations of the compounds, ranging from 0 to 50 μM. 9 titration points were recorded for each compound. The NMR signals from one-dimensional ^{1}H spectra were used to monitor the binding. Each spectrum was recorded using 512 scans. A ^{1}H–^{15}N heteronuclear single quantum coherence (HSQC) spectrum was also recorded for ^{15}N-labelled Aβ42 in the presence of 10 μM **C16**. The HSQC spectrum was recorded overnight, for 240 scans, with a spectral width of 25 ppm (^{15}N offset at 117.5 ppm). All spectra were obtained using a 18.8 T (800 MHz ^{1}H frequency) Avance III HD Bruker spectrometer equipped with a cryoprobe.

Supporting Information

Supplementary methods detailing synthesis of perphenazine conjugates, characterisation by nuclear magnetic resonance spectroscopy and screening using synthetic Aβ42, supporting figures S1–S16, statistical results for the one-way ANOVAs presented in Figure 3 (tables S5–S9), rate constants and mean squared errors from presented fits of ThT fluorescence data and effective monomer concentrations used for Figure 5 (tables S8–S12), SI references.

Acknowledgements

The work was funded by Australian Research Council Discovery Project grant (DP200102463) to MS, AK and PJR. SRB, JSPA and MAS were supported by Research Training Program Scholarships from the Australian Government (Department of Education, Skills and Employment). MK, MAS and ELW's research is supported by the National Health and Medical Research Council of Australia (NHMRC; APP1132524). MK is an NHMRC Principal Research Fellow (APP1154692). MRZ acknowledges support from the Herchel Smith Fund. The authors thank Elva (Meng) Shi and Dr Malcolm Spain for assistance with synthesis and characterisation of compounds and Dr Bill Bubb for comments on the manuscript. The authors acknowledge the facilities and the scientific and technical assistance of staff within the Sydney Analytical and Sydney Microscopy & Microanalysis Core Research Facilities at the University of Sydney. We acknowledge and pay respect to the Gadigal people of the Eora Nation, the traditional owners of the land on which we research, teach, and collaborate at the University of Sydney.

Author Contributions

S.R.B., J.S.P.A., M.A.S., M.R.Z., V.L., M.S-H., F.J., A.H.K., T.P.J.K., G.M., E.L.W., M.H.T., P.J.R. and M.S. conceived the study and developed the methodology. S.R.B., J.S.P.A., M.A.S., V.L., M.S-H., A.D.J.M. and F.J. generated the data. S.R.B., M.A.S., M.R.Z., M.S-H. and G.M. performed the data analysis. A.H.K., T.P.J.K., E.L.W., M.K., M.H.T., P.J.R. and M.S. were involved in supervision. M.K., P.J.R. and M.S. provided resources. S.R.B., J.S.P.A., M.A.S., P.J.R. and M.S. wrote the first draft of the manuscript. All authors reviewed the final manuscript and provided editorial advice.

Additional Information

Conflicts of interest

There are no conflicts of interest to declare.

References

1. Benilova, I., Karran, E., and De Strooper, B. (2012) The toxic Aβ oligomer and Alzheimer's disease: an emperor in need of clothes, *Nature neuroscience 15*, 349-357.
2. Heller, G. T., Aprile, F. A., Michaels, T. C. T., Limbocker, R., Perni, M., Ruggeri, F. S., Mannini, B., Löhr, T., Bonomi, M., Camilloni, C., De Simone, A., Felli, I. C., Pierattelli, R., Knowles, T. P. J., Dobson, C. M., and Vendruscolo, M. (2020) Small-molecule sequestration of amyloid-β as a drug discovery strategy for Alzheimer's disease, *Science Advances 6*, eabb5924.
3. Michaels, T. C. T., Šarić, A., Curk, S., Bernfur, K., Arosio, P., Meisl, G., Dear, A. J., Cohen, S. I. A., Dobson, C. M., Vendruscolo, M., Linse, S., and Knowles, T. P. J. (2020) Dynamics of oligomer populations formed during the aggregation of Alzheimer's Aβ42 peptide, *Nature Chemistry 12*, 445-451.
4. Chiti, F., and Dobson, C. M. (2009) Amyloid formation by globular proteins under native conditions, *Nature chemical biology 5*, 15-22.
5. Lee, S. J. C., Nam, E., Lee, H. J., Savelieff, M. G., and Lim, M. H. (2017) Towards an understanding of amyloid-β oligomers: characterization, toxicity mechanisms, and inhibitors, *Chemical Society Reviews 46*, 310-323.
6. Fantini, J., Chahinian, H., and Yahi, N. (2020) Progress toward Alzheimer's disease treatment: Leveraging the Achilles' heel of Aβ oligomers?, *Protein Science 29*, 1748-1759.
7. Banerjee, S., Hashemi, M., Zagorski, K., and Lyubchenko, Y. L. (2021) Cholesterol in Membranes Facilitates Aggregation of Amyloid β Protein at Physiologically Relevant Concentrations, *ACS Chem Neurosci 12*, 506-516.
8. Jadiya, P., Kolmetzky, D. W., Tomar, D., Di Meco, A., Lombardi, A. A., Lambert, J. P., Luongo, T. S., Ludtmann, M. H., Praticò, D., and Elrod, J. W. (2019) Impaired mitochondrial calcium efflux contributes to disease progression in models of Alzheimer's disease, *Nature communications 10*, 3885.
9. Tsigelny, I. F., Sharikov, Y., Kouznetsova, V. L., Greenberg, J. P., Wrasidlo, W., Gonzalez, T., Desplats, P., Michael, S. E., Trejo-Morales, M., Overk, C. R., and Masliah, E. (2014) Structural diversity of Alzheimer's disease amyloid-β dimers and their role in oligomerization and fibril formation, *Journal of Alzheimer's disease : JAD 39*, 583-600.
10. Lee, A., Kondapalli, C., Virga, D. M., Lewis, T. L., Jr., Koo, S. Y., Ashok, A., Mairet-Coello, G., Herzig, S., Foretz, M., Viollet, B., Shaw, R., Sproul, A., and Polleux, F. (2022) Aβ42 oligomers trigger synaptic loss through CAMKK2-AMPK-dependent effectors coordinating mitochondrial fission and mitophagy, *Nature communications 13*, 4444.
11. Zott, B., Simon, M. M., Hong, W., Unger, F., Chen-Engerer, H.-J., Frosch, M. P., Sakmann, B., Walsh, D. M., and Konnerth, A. (2019) A vicious cycle of β amyloid–dependent neuronal hyperactivation, *Science 365*, 559-565.
12. Cohen, S. I. A., Linse, S., Luheshi, L. M., Hellstrand, E., White, D. A., Rajah, L., Otzen, D. E., Vendruscolo, M., Dobson, C. M., and Knowles, T. P. J. (2013) Proliferation of amyloid-β42 aggregates occurs through a secondary nucleation mechanism, *Proceedings of the National Academy of Sciences 110*, 9758-9763.
13. Gillam, J. E., and MacPhee, C. E. (2013) Modelling amyloid fibril formation kinetics: mechanisms of nucleation and growth, *Journal of physics. Condensed matter : an Institute of Physics journal 25*, 373101.
14. Linse, S. (2017) Monomer-dependent secondary nucleation in amyloid formation, *Biophys Rev 9*, 329-338.
15. Serra-Batiste, M., Ninot-Pedrosa, M., Bayoumi, M., Gairí, M., Maglia, G., and Carulla, N. (2016) Aβ42 assembles into specific β-barrel pore-forming oligomers in membrane-mimicking environments, *Proceedings of the National Academy of Sciences 113*, 10866-10871.

16. Michaels, T. C. T., Šarić, A., Meisl, G., Heller, G. T., Curk, S., Arosio, P., Linse, S., Dobson, C. M., Vendruscolo, M., and Knowles, T. P. J. (2020) Thermodynamic and kinetic design principles for amyloid-aggregation inhibitors, *Proceedings of the National Academy of Sciences*, 202006684.
17. Habchi, J., Arosio, P., Perni, M., Costa, A. R., Yagi-Utsumi, M., Joshi, P., Chia, S., Cohen, S. I. A., Müller, M. B. D., Linse, S., Nollen, E. A. A., Dobson, C. M., Knowles, T. P. J., and Vendruscolo, M. (2016) An anticancer drug suppresses the primary nucleation reaction that initiates the production of the toxic Aβ42 aggregates linked with Alzheimer's disease, *Science Advances 2*, e1501244.
18. Ikenoue, T., Aprile, F. A., Sormanni, P., and Vendruscolo, M. (2021) Rationally Designed Bicyclic Peptides Prevent the Conversion of Aβ42 Assemblies Into Fibrillar Structures, *Front Neurosci 15*, 623097.
19. Habchi, J., Chia, S., Limbocker, R., Mannini, B., Ahn, M., Perni, M., Hansson, O., Arosio, P., Kumita, J. R., Challa, P. K., Cohen, S. I. A., Linse, S., Dobson, C. M., Knowles, T. P. J., and Vendruscolo, M. (2017) Systematic development of small molecules to inhibit specific microscopic steps of Aβ42 aggregation in Alzheimer's disease, *Proceedings of the National Academy of Sciences 114*, E200-E208.
20. Limbocker, R., Chia, S., Ruggeri, F. S., Perni, M., Cascella, R., Heller, G. T., Meisl, G., Mannini, B., Habchi, J., Michaels, T. C. T., Challa, P. K., Ahn, M., Casford, S. T., Fernando, N., Xu, C. K., Kloss, N. D., Cohen, S. I. A., Kumita, J. R., Cecchi, C., Zasloff, M., Linse, S., Knowles, T. P. J., Chiti, F., Vendruscolo, M., and Dobson, C. M. (2019) Trodusquemine enhances Aβ42 aggregation but suppresses its toxicity by displacing oligomers from cell membranes, *Nature communications 10*, 225.
21. Ettcheto, M., Cano, A., Manzine, P. R., Busquets, O., Verdaguer, E., Castro-Torres, R. D., García, M. L., Beas-Zarate, C., Olloquequi, J., Auladell, C., Folch, J., and Camins, A. (2020) Epigallocatechin-3-Gallate (EGCG) Improves Cognitive Deficits Aggravated by an Obesogenic Diet Through Modulation of Unfolded Protein Response in APPswe/PS1dE9 Mice, *Molecular neurobiology 57*, 1814-1827.
22. Cataldi, R., Chia, S., Pisani, K., Ruggeri, F. S., Xu, C. K., Šneideris, T., Perni, M., Sarwat, S., Joshi, P., Kumita, J. R., Linse, S., Habchi, J., Knowles, T. P. J., Mannini, B., Dobson, C. M., and Vendruscolo, M. (2021) A dopamine metabolite stabilizes neurotoxic amyloid-β oligomers, *Communications biology 4*, 19-19.
23. Zhong, X., Kumar, R., Wang, Y., Biverstål, H., Ingeborg Jegerschöld, C., P, J. B. K., Johansson, J., Abelein, A., and Chen, G. (2022) Amyloid Fibril Formation of Arctic Amyloid-β 1-42 Peptide is Efficiently Inhibited by the BRICHOS Domain, *ACS Chem Biol*.
24. Munke, A., Persson, J., Weiffert, T., De Genst, E., Meisl, G., Arosio, P., Carnerup, A., Dobson, C. M., Vendruscolo, M., Knowles, T. P. J., and Linse, S. (2017) Phage display and kinetic selection of antibodies that specifically inhibit amyloid self-replication, *Proceedings of the National Academy of Sciences 114*, 6444.
25. Liu, H., Yu, L., Dong, X., and Sun, Y. (2017) Synergistic effects of negatively charged hydrophobic nanoparticles and (−)-epigallocatechin-3-gallate on inhibiting amyloid β-protein aggregation, *Journal of Colloid and Interface Science 491*, 305-312.
26. Palhano, F. L., Lee, J., Grimster, N. P., and Kelly, J. W. (2013) Toward the molecular mechanism(s) by which EGCG treatment remodels mature amyloid fibrils, *Journal of the American Chemical Society 135*, 7503-7510.
27. Young, L. M., Saunders, J. C., Mahood, R. A., Revill, C. H., Foster, R. J., Tu, L.-H., Raleigh, D. P., Radford, S. E., and Ashcroft, A. E. (2015) Screening and classifying small-molecule inhibitors of amyloid formation using ion mobility spectrometry–mass spectrometry, *Nature Chemistry 7*, 73-81.
28. Zhu, L., Song, Y., Cheng, P.-N., and Moore, J. S. (2015) Molecular Design for Dual Modulation Effect of Amyloid Protein Aggregation, *Journal of the American Chemical Society 137*, 8062-8068.
29. Tamanini, E., Flavin, K., Motevalli, M., Piperno, S., Gheber, L. A., Todd, M. H., and Watkinson, M. (2010) Cyclam-Based "Clickates": Homogeneous and Heterogeneous Fluorescent Sensors for Zn(II), *Inorganic Chemistry 49*, 3789-3800.

30. Wong, J. K.-H., Ast, S., Yu, M., Flehr, R., Counsell, A. J., Turner, P., Crisologo, P., Todd, M. H., and Rutledge, P. J. (2016) Synthesis and Evaluation of 1,8-Disubstituted-Cyclam/Naphthalimide Conjugates as Probes for Metal Ions, *ChemistryOpen 5*, 375-385.
31. Risacher, S. L., Fandos, N., Romero, J., Sherriff, I., Pesini, P., Saykin, A. J., and Apostolova, L. G. (2019) Plasma amyloid beta levels are associated with cerebral amyloid and tau deposition, *Alzheimer's & dementia (Amsterdam, Netherlands) 11*, 510-519.
32. Linse, S. (2020) Expression and Purification of Intrinsically Disordered Aβ Peptide and Setup of Reproducible Aggregation Kinetics Experiment, *Methods in molecular biology (Clifton, N.J.) 2141*, 731-754.
33. Walsh, D. M., Thulin, E., Minogue, A. M., Gustavsson, N., Pang, E., Teplow, D. B., and Linse, S. (2009) A facile method for expression and purification of the Alzheimer's disease-associated amyloid beta-peptide, *The FEBS journal 276*, 1266-1281.
34. House, E., Collingwood, J., Khan, A., Korchazkina, O., Berthon, G., and Exley, C. (2004) Aluminium, iron, zinc and copper influence the in vitro formation of amyloid fibrils of Abeta42 in a manner which may have consequences for metal chelation therapy in Alzheimer's disease, *Journal of Alzheimer's disease : JAD 6*, 291-301.
35. Lee, M.-C., Yu, W.-C., Shih, Y.-H., Chen, C.-Y., Guo, Z.-H., Huang, S.-J., Chan, J. C. C., and Chen, Y.-R. (2018) Zinc ion rapidly induces toxic, off-pathway amyloid-β oligomers distinct from amyloid-β derived diffusible ligands in Alzheimer's disease, *Scientific Reports 8*, 4772.
36. Mold, M., Ouro-Gnao, L., Wieckowski, B. M., and Exley, C. (2013) Copper prevents amyloid-β1–42 from forming amyloid fibrils under near-physiological conditions in vitro, *Scientific Reports 3*, 1256.
37. Haass, C., and Selkoe, D. J. (2007) Soluble protein oligomers in neurodegeneration: lessons from the Alzheimer's amyloid β-peptide, *Nature Reviews Molecular Cell Biology 8*, 101-112.
38. Walsh, D. M., Klyubin, I., Fadeeva, J. V., Cullen, W. K., Anwyl, R., Wolfe, M. S., Rowan, M. J., and Selkoe, D. J. (2002) Naturally secreted oligomers of amyloid beta protein potently inhibit hippocampal long-term potentiation in vivo, *Nature 416*, 535-539.
39. Krishtal, J., Bragina, O., Metsla, K., Palumaa, P., and Tõugu, V. (2017) In situ fibrillizing amyloid-beta 1-42 induces neurite degeneration and apoptosis of differentiated SH-SY5Y cells, *PLOS ONE 12*, e0186636.
40. Cohen, S. I., Vendruscolo, M., Welland, M. E., Dobson, C. M., Terentjev, E. M., and Knowles, T. P. (2011) Nucleated polymerization with secondary pathways. I. Time evolution of the principal moments, *The Journal of chemical physics 135*, 065105.
41. Knowles, T. P. J., Waudby, C. A., Devlin, G. L., Cohen, S. I. A., Aguzzi, A., Vendruscolo, M., Terentjev, E. M., Welland, M. E., and Dobson, C. M. (2009) An Analytical Solution to the Kinetics of Breakable Filament Assembly, *Science 326*, 1533-1537.
42. Meisl, G., Kirkegaard, J. B., Arosio, P., Michaels, T. C., Vendruscolo, M., Dobson, C. M., Linse, S., and Knowles, T. P. (2016) Molecular mechanisms of protein aggregation from global fitting of kinetic models, *Nature protocols 11*, 252-272.
43. Roche, J., Shen, Y., Lee, J. H., Ying, J., and Bax, A. (2016) Monomeric Aβ(1-40) and Aβ(1-42) Peptides in Solution Adopt Very Similar Ramachandran Map Distributions That Closely Resemble Random Coil, *Biochemistry 55*, 762-775.
44. Necula, M., Kayed, R., Milton, S., and Glabe, C. G. (2007) Small molecule inhibitors of aggregation indicate that amyloid beta oligomerization and fibrillization pathways are independent and distinct, *J Biol Chem 282*, 10311-10324.
45. Horsley, J. R., Jovcevski, B., Wegener, K. L., Yu, J., Pukala, T. L., and Abell, A. D. (2020) Rationally designed peptide-based inhibitor of Aβ42 fibril formation and toxicity: a potential therapeutic strategy for Alzheimer's disease, *The Biochemical journal 477*, 2039-2054.
46. Bieschke, J., Russ, J., Friedrich, R. P., Ehrnhoefer, D. E., Wobst, H., Neugebauer, K., and Wanker, E. E. (2010) EGCG remodels mature α-synuclein and amyloid-β fibrils and reduces cellular toxicity, *Proceedings of the National Academy of Sciences 107*, 7710-7715.

679 47. Ehrnhoefer, D. E., Bieschke, J., Boeddrich, A., Herbst, M., Masino, L., Lurz, R., Engemann, S.,
680 Pastore, A., and Wanker, E. E. (2008) EGCG redirects amyloidogenic polypeptides into unstructured,
681 off-pathway oligomers, *Nature Structural & Molecular Biology 15*, 558-566.
682 48. Löhr, T., Kohlhoff, K., Heller, G. T., Camilloni, C., and Vendruscolo, M. (2022) A Small Molecule
683 Stabilizes the Disordered Native State of the Alzheimer's Aβ Peptide, *ACS Chem Neurosci 13*, 1738-
684 1745.
685 49. Spain, M., Wong, J. K. H., Nagalingam, G., Batten, J. M., Hortle, E., Oehlers, S. H., Jiang, X. F.,
686 Murage, H. E., Orford, J. T., Crisologo, P., Triccas, J. A., Rutledge, P. J., and Todd, M. H. (2018)
687 Antitubercular Bis-Substituted Cyclam Derivatives: Structure–Activity Relationships and in Vivo
688 Studies, *Journal of Medicinal Chemistry 61*, 3595-3608.

689